ORIGINAL ARTICLE

Improvement of Basal Ganglia Detectability in Brain Single Photon Emission Computerized Tomography by Wavelet Transformation in Image Processing Domain: A XCAT Phantom Study

Marzie Saeidikia [1], Hadi Seyedarabi [2], Babak Mahmoudian [3], Jalil Pirayesh Islamian [1*]

[1] *Department of Medical Physics, School of Medicine, Tabriz University of Medical Sciences, Tabriz, Iran*

[2] *Faculty of Electrical and Computer Engineering, University of Tabriz, Tabriz, Iran*

[3] *Department of Nuclear Medicine, Tabriz University of Medical Sciences, Tabriz, Iran*

*Corresponding Author: Jalil Pirayesh Islamian
Email: pirayeshj@gmail.com

Received: 17 November 2022 / Accepted: 16 January 2023

Abstract

Purpose: Noise in brain Single Photon Emission Computed Tomography (SPECT) images limits an early diagnosis of Parkinson's Disease (PD). To overcome the limitation, as an image processing approach, wavelet transformation was used to denoising the images also with a segmentation method to differentiate the basal ganglia in brain SPECT.

Materials and Methods: The brain scans of the human 4D Extended Cardiac Torso (XCAT) phantom through the Simulating Medical Imaging Nuclear Detectors (SIMIND) simulated SPECT system were imported to the MATLAB toolkit for image processing. The reconstructed brain images by iterative reconstruction were de-noised through 9 methods of wavelet transformation at different levels, and then six segmentation methods were applied to differentiate the caudate and putamen. The Dice coefficient, Specificity, and Sensitivity evaluation criteria were calculated based on the adaptive thresholding of the selected images from the segmentations. A ground truth image was manually marked by a clinical nuclear medicine specialist.

Results: The dice coefficient was obtained in a range from 0.3979 to 0.6299, as well as the specificity criterion from 0.7682 to 0.8168 and the sensitivity from 0.9049 to 0.9871.

The results from adaptive threshold segmentation and the evaluation criteria showed that the best levels of the nucleuses detectability were provided by level 7 of Biorthogonal, levels 4 and 7 of Coiflet, level 6 of Daubechies, level 5 of Haar, level 6 of Morlet and level 6 of Symlet methods.

Conclusion: Parkinson’s disease may be diagnosed in the early stage by an image processing approach to improve the quality of brain SPECT images.

Keywords: Parkinson’s Disease; Single Photon Emission Computed Tomography; Simulating Medical Imaging Nuclear Detectors; Monte Carlo; Wavelet Transformation; Segmentation.

DOI: https://doi.org/10.18502/fbt.v11i2.15335

1. Introduction

Parkinson's Disease (PD) is a common neurological disorder that happens due to damage to the dopaminergic nigrostriatal system and nerve terminals, involving the central nervous system in the brain [1, 2]. Clinical appearances of the disease are resting tremor, rigidity, and bradykinesia [3]. An early and absolute diagnosis of PD may cause successful management of the disease [4].

There are some medical imaging approaches to diagnose PD by acquiring important structural and functional information about the brain [5]. These modalities include Positron Emission Tomography (PET), Single Photon Emission Computed Tomography (SPECT), Magnetic Resonance Imaging (MRI), and Transcranial Sonography (TCS). Nuclear medicine imaging technology, including SPECT and PET, is widely used as a diagnostic tool to demonstrate the dysfunction of the striatal dopamine terminal and so progression level of PD [6, 7].

Although there are various challenges in front of the PET technique, including limitations in public health system accessibility and high costs [8], the modalities are accounted as sensitive and general imaging methods. Meanwhile, SPECT is less expensive and more accessible than PET; furthermore radiotracers of SPECT have the both benefits of a longer half-life and do not need to be produced and used simultaneously in the same place [9]. In this regard, there were some studies to help early diagnosis of PD using SPECT [2].

To detect even the early stages of PD, Pahuja *et al.*, have proposed the recent neuroimaging techniques such as dopaminergic imaging by SPECT [10]. They proposed that Support Vector Machine (SVM) classification can be used to classify the parts of a patient's brain that were affected by Parkinson's disease at the early stage.

It was shown that ^{99m}Tc-TRODAT-1 radiotracer, by binding to the dopamine transporter, could be used in the dopaminergic imaging system [5]. Hence, a reduction in radiopharmaceutical uptake or striatal Dopamine Transporter (DAT) density account for an indication of the dopaminergic degenerative disorder, including PD [11]. Moreover, SPECT imaging has the advantages of dissociating PD from essential tremors, using 123I-Ioflupane, or from drug-induced Parkinsonism [2]. When image quality plays a vital role in an exact diagnosis of the diseases, some studies using image processing methods were used to improve basal ganglia detectability in brain SPECT. Aprajita Sharma *et al.*, have implemented a Self-Organizing Map (SOM) algorithm for clustering purposes, which classifies all the image pixels to identify the classes of normal and PD situations [12].

Wavelet Transformation (WT) is a mathematical method to separate image signals into different frequency components in discrete and continuous modalities [13]. Over the past few years, wavelet transform has become one of the most potent tools for removing image noise [14].

Borsdorf *et al.*, in a study on image denoising, defined a threshold value in the wavelet field based on the relationship between two images. Then, the reverse results of the wavelet transformation were a denoised image that included all the associated structures [15].

It seems that different types of wavelets and their compatibility with real signals and the low complexity of computing have made the wavelet to be used as an efficient tool in the image processing domain.

Alafeef *et al.*, have used a continuous wavelet transform complex plot to diagnose idiopathic Parkinson's disease. In this study, the denoised brain SPECT image was filtered with continuous wavelet transform, then the target areas were marked as an ellipse to classify artificial neural networks. An accuracy of 97.6% was obtained for diagnosing the affected regions by PD [16].

The aim of the present study was to obtain an optimal noise removal algorithm followed by basal ganglia segmentation to improve the differentiation of caudate and putamen nuclei in brain SPECT. To improve the quality of radioisotope images of the putamen and caudate nuclei in brain SPECT prepared by Simulating Medical Imaging Nuclear Detectors (SIMIND) Monte Carlo program [17], the reconstructed brain images were processed with wavelet transformation in the MATLAB toolkit.

2. Materials and Methods

2.1. Human Phantom

The voxelized 4D extended Cardiac-Torso (XCAT) human phantom was used to produce human brain structures, including the main components of the basal ganglia including putamen and caudate nuclei [18]. The activity ratios of the glands were set to the normal brain as well as reduced activity of PD and then the output files, including attenuation and activity maps, were produced to use in SIMIND simulated brain SPECT.

2.2. SPECT

A Siemens E.CAM gamma camera with a 59.1 × 44.5 × 0.953 cm NaI (Tl) crystal equipped with a Low Energy High Resolution (LEHR) collimator was simulated by the SIMIND Monte Carlo program [19]. The brain SPECT parameters were set with matrix size of 128 × 128, zoom factor of 1.3, 128 projections, and 360° counter-clockwise circular scan head rotation.

An iterative reconstruction algorithm was used to reconstruct the produced projections with 12 iterations and 4 subunits. The reconstructed image with normal radiopharmaceutical absorption was used to perform the image processing process, i.e. denoising and segmentation (Figure 1a). A clinical nuclear medicine specialist defined the region of caudate and putamen nucleus manually on the main image as a ground truth (Figure 1b).

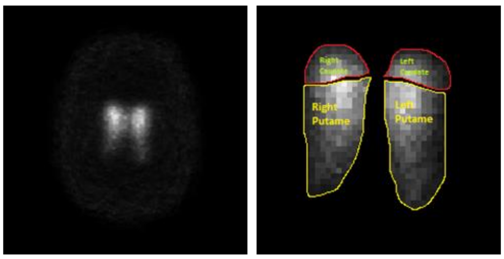

Figure 1. a) A cross-sectional image of the putamen and caudate from XCAT brain SPECT (MLEM iteratively reconstructed with 12 iterations, 4 subunits, 128 × 128 matrix size). The activity ratios of brain background, caudate, and putamen were set to 1, 75, and 75, respectively. b) A ground truth was produced by defining the region of caudate and putamen nucleus in a reconstructed image of brain SPECT by a clinical nuclear medicine specialist

2.3. Image Processing

The reconstructed normal brain images were utilized as input to wavelet transformation.

2.3.1. Discrete Wavelet Transformation

Discrete Wavelet Transformation (DWT) was used to investigate the efficiency of different denoising methods through Equation 1 [13].

$$DWT_x(u,v) = \frac{1}{\sqrt{a_0^u}} \sum_v X(v)\psi\left(\frac{t - v a_0^u b_0}{a_0^u}\right) \qquad (1)$$

Noise in the original images was removed using different wavelet methods including Biorthogonal, Coiflets, Daubechies, Gabor, Gaussian, Haar, Mexican Hat, Morlet, and Symlets [15, 20, 21].

Wavelet analysis of the images was performed in seven levels with a defined threshold for each level. It's worth mentioning that only the Gabor method included four angular parameters.

2.3.2. Segmentation

The binarized image by thresholding, Grayscale intensity difference, Otsu method, Adaptive threshold, active contour, and boundaries of segmentation were used [22-24]. Then, the cropped image of the same area of the original images and the denoising output of the images following zooming were used [25].

Finally, the approved images by a clinical nuclear medicine physician were used to calculate the evaluation criteria.

2.3.3. Evaluation Criteria

Evaluation criteria included Dice Coefficient, Specificity, and Sensitivity [26].

a) Dice Coefficient

Dice Similarity Coefficient (Dice or DSC) criteria were used to calculate the similarity measure of two images (Formula 2).

$$Dice = \frac{2 * TP}{2 * TP + FP + FN} \qquad (2)$$

b) Specificity

Formula 3 was used to calculate specificity:

$$Specificity = \frac{TN}{TN + FP} \qquad (3)$$

c) Sensitivity

Formula 4 was used to obtain sensitivity [26]:

$$Sensitivity = \frac{TP}{TP + FN} \qquad (4)$$

Where TP Indicates the number of instances whose actual category is positive, and the classifier algorithm correctly identifies the category as positive. TN Indicates the number of cases whose basic category is negative, and the classifier algorithm correctly identifies the type as negative. FP indicates the number of instances whose actual category is negative and the category classifier algorithm has erroneously detected as positive. FN indicates the number of instances whose actual class is positive, and the category classifier algorithm has erroneously detected as negative [27].

3. Results

The processed reconstructed brain SPECT images were analyzed visually by two experts in the field of clinical nuclear medicine and also quantitatively by the image processing approaches, including the values of Dice Coefficient, Specificity, and Sensitivity criteria, the efficiency of denoising methods and adaptive thresholding segmentation for the ganglia detectability. The results of the nine wavelet and the six segmentation methods were provided in Table 1. The best levels of the methods were determined by a clinical nuclear medicine specialist and also by an expert in the field of image processing.

According to the specialists on the processed images, Level 7 of the Biorthogonal, levels 4 and 7 of Coiflet, level 6 of Daubechies, level 5 of Haar, level 6 of Morlet, and level 6 of Symlet methods were selected as optimized levels (Figure 2).

4. Discussion

In the present study, to improve the quality of radioisotope images of the putamen and caudate nuclei in the human XCAT brain SPECT prepared by the SIMIND Monte Carlo simulation [17], the reconstructed images were processed with wavelet transformation in the MATLAB toolkit, including de-noising through 9 methods of wavelet transformation at different levels, and six segmentation methods. Comparing the results from the adaptive threshold segmentation along with the evaluation criteria, the best levels of detectability for the nuclei provided by level 7 of the Biorthogonal method, levels 4 and 7 of the Coiflet method, level 6 of the Daubechies method, level 5 of the Haar method, level 6 of the Morlet method and level 6 of the Symlet method (Figure 2).

Figure 3 represents the average values of evaluation criteria, including sensitivity, specificity, and Dice coefficient on detectability of the putamen and caudate nucleus by Biorthogonal, Coiflet, Daubechies, Haar, Morlet, and Symlet methods.

Considering that this is the first study to combine such denoising and segmentation methods for the analysis of brain SPECT images, there are comparisons to be made with other PD-related studies or studies that use the segmentation method for other imaging modalities.

Borsdorf *et al.*, [15], using the inverse wavelet transform, denoised the lung image obtained through X-ray imaging while preserving all its relevant structures.

Our results also on denoising the images of caudate and putamen glands using nine wavelet methods confirmed their findings. The difference in noise reduction levels may be related to the different imaging methods and the anatomical areas of studies.

Pahuja *et al.*, have suggested dopaminergic imaging techniques such as SPECT imaging to detect PD in the early stages. In this research, SVM classification was used to classify parts of the patient's brain that are affected by Parkinson's disease. They reported specificity and sensitivity measures of 0.931 and 0.986, respectively [10].

The specificity and sensitivity measures of our study with a similar method for processing SPECT radioisotopic images are in agreement.

Abdallah *et al.*, have used watershed segmentation to determine the Gross Tumor Volume (GTVs) of malignant tumors on brain MRI images in the MATLAB toolkit. GTVs were manually identified as ground truth [28]. The Dice, Sensitivity, and Specificity coefficients were calculated to be 0.86 ± 0.03, 0.94 ± 0.06, 0.90 ± 0.09, respectively. The differences in Dice coefficient and Specificity of our results (Figure 2) may be due to differences in the inherent quality of MRI and SPECT images as well as some discrepancies in the watershed and adaptive threshold segmentation methods. In this regard, Bahadure *et al.*, used the Berkeley Wavelet Transform (BWT) segmentation method by the SVM classification model method to identify and diagnose the tumor on MRI images [29]. Their results on the effectiveness of the proposed method for detecting normal and abnormal brain tissue in MRI images also provided the accuracy, Specificity, Sensitivity, and mean Dice measures of 96.51%, 94.2%, 97.72%, and 0.82, respectively.

In another research by Sakalauskas *et al.*, a transcranial Ultrasonographic (US) image analysis system was

Table 1. Results on the evaluation criteria of Wavelet methods from Adaptive Threshold segmentation for differentiating of the putamen and caudate nuclei in reconstructed brain XCAT phantom SPECT images

Methods	Level	Dice	Specificity	Sensitivity
Biorthogonal	3	0.5311	0.7844	0.9866
	4	0.6009	0.7894	0.9747
	6	0.6012	0.7901	0.9847
	7	0.6171	0.7917	0.9464
	Average ±STD	0.5876±0.0384	0.7889±0.0031	0.9731±0.0185
Coiflet	3	0.4964	0.7839	0.9854
	4	0.5107	0.7898	0.9850
	5	0.4758	0.7834	0.9619
	7	0.5169	0.7892	0.9861
	Average±STD	0.4999±0.0182	0.7865±0.0033	0.9796±0.0118
Daubechies	3	0.47625	0.7843	0.9855
	4	0.4919	0.7890	0.9847
	6	0.5010	0.7869	0.9856
	7	0.4897	0.7871	0.9405
	Average±STD	0.4897±0.0102	0.7868±0.0019	0.9740±0.0223
Haar	1	0.4392	0.7685	0.9814
	2	0.4159	0.7682	0.9773
	4	0.4039	0.7686	0.9831
	5	0.5529	0.8038	0.9637
	6	0.3979	0.7685	0.9817
	Average±STD	0.4420±0.0640	0.7755±0.0158	0.9774±0.0079
Morlet	1	0.5010	0.7871	0.9049
	2	0.4970	0.7848	0.9800
	3	0.4740	0.7836	0.9832
	4	0.5852	0.8087	0.9842
	5	0.5635	0.8033	0.9839
	6	0.6299	0.8168	0.9696
	7	0.5555	0.8052	0.9686
	Average±STD	0.5437±0.0555	0.7985±0.0132	0.9677±0.0285
Symlet	6	0.5389	0.7867	0.9835
	7	0.5193	0.7923	0.9871
	Average±STD	0.5291±0.0138	0.7895±0.0039	0.9853±0.0025

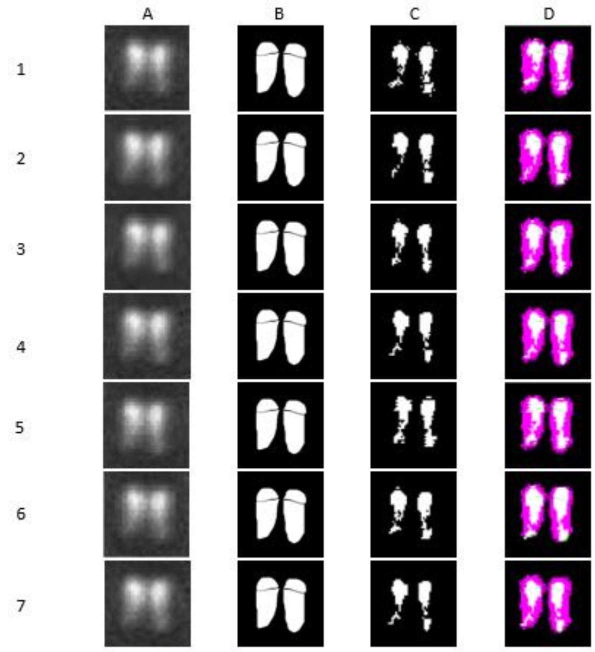

Figure 2. Reconstructed images of brain SPECT, including the putamen and caudate that were processed: (a) Denoised Image, (b) Ground Truth Image, (c) Adaptive Threshold Image, (d) fusion of b and c. The rows from 1 to 6 indicate the levels as below: (1) Level 7 of the Biorthogonal Method, (2) Level 4 of the Coiflet Method, (3) level 7 of the Coiflet Method, (4) Level 6 of the Daubechies Method, (5) Level 5 of the Haar Method, (6) Level 6 of the Morlet Method, and (7) Level 6 of the Symlet Method

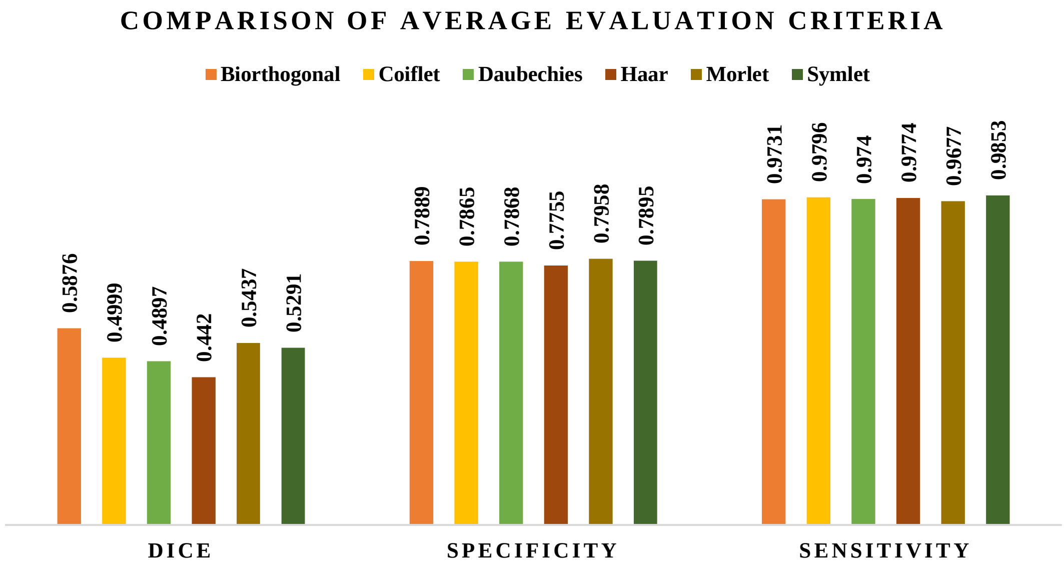

Figure 3. Column charts of the average values of evaluation criteria, including sensitivity, specificity, and Dice coefficient on differentiating putamen and caudate nucleus by Biorthogonal, Coiflet, Daubechies, Haar, Morlet, and Symlet methods

developed to diagnose Parkinson's disease by 64 algorithms on segmenting and evaluating the middle area of the brain and substantia nigra images of 136 patients [30]. They obtained sensitivity and specificity measures of 0.85 and 0.75, respectively, with the method. The main limitation of transcranial image-based diagnosis is the poor low quality of the images in the cranial region of the brain.

5. Conclusion

Image denoising and segmentation by wavelet transformation may be used to improve the detectability of basal ganglia in brain SPECT images for the early detection of Parkinson's disease.

6. Limitations of the Study

It should be mentioned that the inherent low quality of radioisotope images affected by the detector's large size, scattering and attenuation of photons, and the random nature of radioisotope decay was one of the important limitations of present study. Meanwhile, in order to detect or eliminate diagnostic errors on the activity of brain basal ganglia, as suggested in the present study, various activities of the ganglia must be introduced along with the normal uptake, when the ganglia are normal, so any changes of the uptake due to the disease will be explored with details.

Acknowledgments

This study has been supported by the deputy of research at Tabriz University of Medical Sciences, Tabriz, Iran [Grant # 62741].

References

1- TC Booth, M Nathan, AD Waldman, A-M Quigley, AH Schapira, and J Buscombe, "The role of functional dopamine-transporter SPECT imaging in parkinsonian syndromes, part 1." *American Journal of Neuroradiology*, Vol. 36 (No. 2), pp. 229-35, (2015).

2- Seong-Jin Son, Mansu Kim, and Hyunjin Park, "Imaging analysis of Parkinson's disease patients using SPECT and tractography." *Scientific reports*, Vol. 6 (No. 1), pp. 1-11, (2016).

3- Dun-Hui Li, Ya-Chao He, Jun Liu, and Sheng-Di Chen, "Diagnostic accuracy of transcranial sonography of the substantia nigra in Parkinson's disease: a systematic review and meta-analysis." *Scientific reports*, Vol. 6 (No. 1), pp. 1-9, (2016).

4- R Prashanth, Sumantra Dutta Roy, Pravat K Mandal, and Shantanu Ghosh, "Automatic classification and prediction models for early Parkinson's disease diagnosis from SPECT imaging." *Expert Systems with Applications*, Vol. 41 (No. 7), pp. 3333-42, (2014).

5- Payam Sasannezhad *et al.*, "99mTc-TRODAT-1 SPECT imaging in early and late onset Parkinson's disease." *Asia Oceania Journal of Nuclear Medicine and Biology*, Vol. 5 (No. 2), p. 114, (2017).

6- John P Seibyl, "Imaging studies in movement disorders." in *Seminars in nuclear medicine*, (2003), Vol. 33 (No. 2): *Elsevier*, pp. 105-13.

7- David J Brooks, "Imaging approaches to Parkinson disease." *Journal of Nuclear Medicine*, Vol. 51 (No. 4), pp. 596-609, (2010).

8- Ludovico Minati, M Grisoli, F Carella, T De Simone, MG Bruzzone, and M Savoiardo, "Imaging degeneration of the substantia nigra in Parkinson disease with inversion-recovery MR imaging." *American Journal of Neuroradiology*, Vol. 28 (No. 2), pp. 309-13, (2007).

9- Ling Wang, Qi Zhang, Huanbin Li, and Hong Zhang, "SPECT molecular imaging in Parkinson's disease." *Journal of Biomedicine and Biotechnology*, Vol. 2012(2012).

10- Gunjan Pahuja, TN Nagabhushan, and Bhanu Prasad, "Early detection of Parkinson's disease by using SPECT imaging and biomarkers." *Journal of Intelligent Systems*, Vol. 29 (No. 1), pp. 1329-44, (2020).

11- Hiroki Nosaka *et al.*, "Influence of Brain Atrophy using Semi-quantitative Analysis in [123I] FP-CIT Single Photon Emission Computed Tomography: A Monte Carlo Simulation Study." (2021).

12- Aprajita Sharma and Ram Nivas Giri, "An Elegant Approach for Diagnosis of Parkinson's disease on MRI Brain Images by Means of a Neural Network." *International Journal of Engineering Sciences & Research Technology*, Vol. 2 (No. 9), pp. 2553-57, (2013).

13- Mou-Fa Guo, Xiao-Dan Zeng, Duan-Yu Chen, and Nien-Che Yang, "Deep-learning-based earth fault detection using continuous wavelet transform and convolutional neural network in resonant grounding distribution systems." *IEEE Sensors Journal*, Vol. 18 (No. 3), pp. 1291-300, (2017).

14- Arpan Zaeni, Tria Kasnalestari, and Umar Khayam, "Application of wavelet transformation symlet type and coiflet type for partial discharge signals denoising." in *2018 5th International Conference on Electric Vehicular Technology (ICEVT)*, (2018): *IEEE*, pp. 78-82.

15- Anja Borsdorf, Rainer Raupach, Thomas Flohr, and Joachim Hornegger, "Wavelet based noise reduction in CT-images using correlation analysis." *IEEE transactions on medical imaging*, Vol. 27 (No. 12), pp. 1685-703, (2008).

16- Maha Alafeef and Mohammad Fraiwan, "On the diagnosis of idiopathic Parkinson's disease using continuous wavelet transform complex plot." *Journal of Ambient Intelligence and Humanized Computing*, Vol. 10 (No. 7), pp. 2805-15, (2019).

17- Michael Ljungberg, "The SIMIND Monte Carlo program. In: M Ljungberg S E Strand, M A King, editors.

Monte Carlo calculations in nuclear medicine: Applications in diagnostic imaging.” *2nd ed. Boca Raton: CRC Press*; p.111–128, (2012).

18- William Paul Segars, et al., “4D XCAT phantom for multimodality imaging research.” *Medical Physics,* Vol. 37(9):4902-15, (2010).

19- Mohammad Taghi Bahreyni Toossi, et al., “SIMIND Monte Carlo simulation of a single photon emission CT.” *Journal of Medical Physics*, Vol.35(1):42-7, (2010).

20- PMK Prasad and G Umamadhuri, "Biorthogonal wavelet-based image compression." in *Artificial Intelligence and Evolutionary Computations in Engineering Systems*: *Springer*, (2018), pp. 391-404.

21- Rahul Sahu and MP Parsai, "Comparison of digital image denoising method using various Transforms on Satellite Imagery." in *2019 2nd International Conference on Intelligent Computing, Instrumentation and Control Technologies (ICICICT)*, (2019), Vol. 1: *IEEE*, pp. 1391-99.

22- Nihaal Mehta *et al.*, "Impact of binarization thresholding and brightness/contrast adjustment methodology on optical coherence tomography angiography image quantification." *American journal of ophthalmology,* Vol. 205pp. 54-65, (2019).

23- N Senthilkumaran and S Vaithegi, "Image segmentation by using thresholding techniques for medical images." *Computer Science & Engineering: An International Journal*, Vol. 6 (No. 1), pp. 1-13, (2016).

24- Diego Marcos *et al.*, "Learning deep structured active contours end-to-end." in *Proceedings of the IEEE Conference on Computer Vision and Pattern Recognition*, (2018), pp. 8877-85.

25- Yunyi Tang and Yuanpeng Zhu, "Image zooming based on two classes of C1-continuous coons patches construction with shape parameters over triangular domain." *Symmetry,* Vol. 12 (No. 4), p. 661, (2020).

26- Boliang Yu *et al.*, "HybraPD atlas: Towards precise subcortical nuclei segmentation using multimodality medical images in patients with Parkinson disease." *Human brain mapping,* Vol. 42 (No. 13), pp. 4399-421, (2021).

27- Nooshin Nabizadeh and Miroslav Kubat, "Brain tumors detection and segmentation in MR images: Gabor wavelet vs. statistical features." *Computers & Electrical Engineering,* Vol. 45pp. 286-301, (2015).

28- Yousif Abdallah, "Delineation of brain tumours for radiotherapy patients using image segmentation techniques." *Onkologia i Radioterapia,* Vol. 14 (No. 5), pp. 1-5, (2020).

29- Nilesh Bhaskarrao Bahadure, Arun Kumar Ray, and Har Pal Thethi, "Image analysis for MRI based brain tumor detection and feature extraction using biologically inspired BWT and SVM." *International Journal of Biomedical Imaging,* Vol. 2017(2017).

30- Andrius Sakalauskas, Vita Špečkauskienė, Kristina Laučkaitė, Rytis Jurkonis, Daiva Rastenytė, and Arūnas Lukoševičius, "Transcranial ultrasonographic image analysis system for decision support in parkinson disease." *Journal of Ultrasound in Medicine,* Vol. 37 (No. 7), pp. 1753-61, (2018).